Analysis and DSP Implementation of Multisampled Three-Phase Current Controllers

Abstract—This paper presents a method for current control of three-phase systems, realized using the multisampled pulse-width modulator (MS-PWM). The feedback signal is highly oversampled and filtered to obtain its average value with high noise suppression. Independently, the control update rate is chosen to be higher than double the switching frequency, which reduces delays due to calculation and digital modulation. In this way, the proposed strategy offers improved dynamic response compared to standard double-update PWM, while in the same it offers a high quality feedback signal, robust to noise sampling and aliasing. The analysis is verified using a standard digital signal processor TI f28379d and a Typhoon HIL 402 hardware-in-the-loop system that emulates an electric drive with a high-speed BLDC motor.

Index Terms—Current control, Digital pulse-width modulators (DPWM), Multisampled pulse-width modulators (MS-PWM)

I. INTRODUCTION

Field oriented control (FOC) in electrical drives and voltage oriented control (VOC) in grid-connected converters is a well-established strategy for the control of high performance three-phase electrical systems [1]. An essential part of this concept is the inner current control loop, which regulates the synchronous rotating frame (SRF) currents [1]. The SRF controller must provide a decoupling function between d and q axis currents. This is particularly challenging for high-speed or high pole-pair electrical drives, which operate at very high output frequencies [2], [3]. Regarding controller structures, SRF proportional-integral (PI) controllers are most frequently used due to their simplicity and satisfactory performance for the majority of the industrial requirements [2], [4]. However, their transient decoupling capability is rather limited, especially at high output frequencies [5]. Achieving a robust high-frequency operation and high bandwidths has driven the design of current controllers directly in discrete-time domain [5]–[7]. Belonging to this group are the dead-beat current controllers that offer a very fast transient response but at the cost of considerable performance degradation in the presence of variable parameters and measurement errors, which is often the case in control of electric drives [8]–[10]. A more robust operation is achieved with the use of the discrete internal model controller (IMC) design [5]–[7]. This strategy has proven to offer high closed loop bandwidths at very high output frequencies [3], [6], [7].

The demerit of digital control systems is the introduction of delays due to the analog-to-digital conversion (ADC), algorithm execution time, and digital pulse width modulation (DPWM) [11]. These delays limit the achievable bandwidths and impair the decoupling function of SRF current controllers.

In most state-of-the-art applications, double-sampled double-update (DS-DU-PWM) control strategy is used, where the feedback is sampled twice per PWM period, with acquisition instants being synchronized so that the average value is obtained [11]. In industrial applications, the feedback signal is often strongly corrupted by various noise sources, which requires additional filtering [6]. Furthermore, sampling of the average value is compromised by system delays, which causes aliasing problems [11]. Improved error-free feedback acquisition is achieved by oversampling the signal and then averaging it over the PWM period. In this way, the average value is obtained with additional high noise suppression [6], [12]. The filtered signal is then decimated so that the control action is executed with the double-update rate. This kind of strategy, implemented in [6], is here labeled as multi-sampled double-update (MS-DU-PWM) control. The MS-DU-PWM strategy results in a high quality feedback signal, however, it yields a negative impact on the system dynamics. Achieving high bandwidths with the one switching period averaging requires modification of the controller structure, to compensate the introduced phase lag [6]. The delay-related limitations of digital control have inspired investigation of the multisampled PWM (MS-PWM) control, with purpose of enabling analog-like control bandwidths in digital systems. The multisampled multi-update (MS-MU-PWM) approach relies on acquiring the control variables and updating the modulating waveform multiple times per switching period [8], [10], [12]–[17]. The concept of MS-MU-PWM digital control offers a significant delay reduction and is therefore a promising solution for breaking the bandwidth limitations of digital control systems [18]. Besides the small-signal improvement, MS-MU-PWM also provides a nonlinear advantage as the modulating waveform can be updated multiple times per switching period. This yields a lower response delay to large-signal perturbations [14]. On the other hand, MS-MU-PWM introduces a set of nonlinearities, mainly due to the modulating waveform discontinuity and the switching ripple is introduced in the feedback [13], [16]. For this reason, most of the reported MS-MU-PWM methods include digital filtering, such as moving average filters (MAFs), to completely remove the switching ripple [15], [17].

This paper analyzes the use of the digital MS-MU-PWM IMC-based current controller, suitable for implementation on standard DSP platforms. The main goal of the paper is to analyze the performance of MS-MU-PWM with one switching period averaging and to compare it with standardly used DS-DU-PWM and MS-DU-PWM methods. The target is to
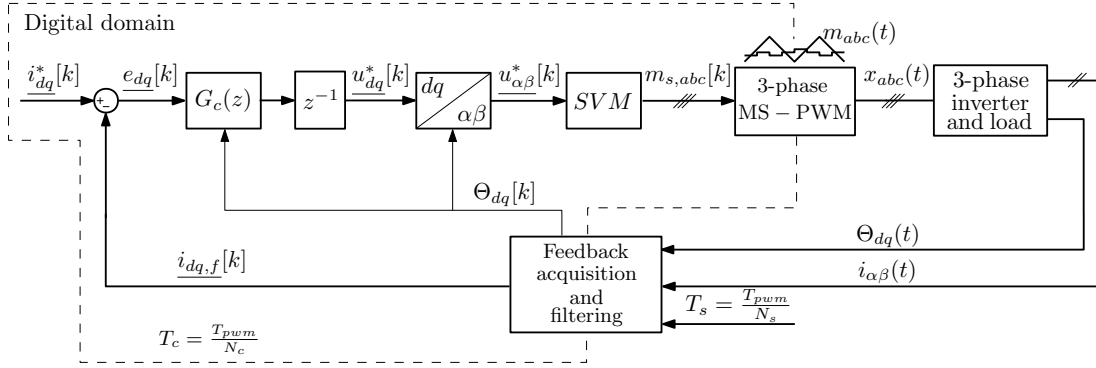
Fig. 1: Multisampled control loop of a three-phase current-controlled inverter. The feedback acquisition and filtering is explained in subsection III A.

show that the MS-MU-PWM control with feedback averaging provides an improved dynamic performance compared to DS-DU-PWM, while offering a high quality feedback signal in the same manner as MS-DU-PWM.

This paper is organized as follows. Section II explains the multi-rate control structure and emphasizes benefits of MS-MU-PWM control. Subsequently, the discrete-time model of a three-phase RL load is derived and used to obtain a model-based controller structure. Section III focuses on the implementation of multisampled feedback acquisition, filtering, and choice of the control update rate. In section IV, the controller gains are chosen for a suitable comparison between DS-DU, MS-DU, and MS-MU methods. The discrete-time modeling is verified using the sweep frequency response analysis. Section V provides experimental verification on the TI DSP f28379d and a hardware-in-the-loop emulation of a BLDC electric drive. The conclusions of the study are drawn in Section VI.

II. MULTI-RATE CONTROL SYSTEM

The multi-rate control system of a three-phase RL load in dq frame is shown in Fig. 1. The system can be separated into digital and continuous-time domain. An ADC is used to transform feedback signal from analog to digital domain. This action is performed with a sampling frequency $f_s = N_s f_{pwm}$, where N_s is the multisampling (oversampling) factor and f_{pwm} is the switching frequency of the inverter. The digital domain operates with frequency $f_c = N_c f_{pwm}$, where N_c is the multi-update factor that determines the update rate of the controller output. The choice of this frequency is independent of the sampling frequency, as the feedback signal can be oversampled with frequency f_s and then filtered and decimated to control frequency f_c. The digital domain is comprised of feedback filter $G_{fb}(z)$, controller $G_c(z)$, coordinate frame transformation block, and space vector modulation (SVM) block. The controller $G_c(z)$ outputs reference voltage in dq frame, $\underline{u_{dq}}^*[k]$, which is then transformed to $\alpha\beta$ frame. This reference voltage is used to obtain digital modulating waveform for each inverter phase, $m_{s,abc}[k]$. Conversion from digital to analog domain is performed by MS-PWM. Its inherent zero-order hold function transforms the digital impulse train $m_{s,abc}[k]$ into the continuous-time modulating waveform

$m_{abc}(t)$. MS-PWM with the triangular carrier is used due to its favorable characteristics in MS-MU-PWM control [13]. The PWM output is used as a gate signal $x_{abc}(t)$. The three-phase inverter is used to supply a generic RL load, which can model either an AC electrical machine or the electrical grid. The sensed feedback includes line currents $i_{\alpha\beta}(t)$ and the angle of the dq coordinate frame Θ_{dq}.

A. Motivation behind MS-MU-PWM control

Modern processors feature high computational power, which enables short execution times for control routines. However, switching frequencies of power converters are hardware limited, and do not go over several tens of kHz for medium power applications. This hardware based limitation directly affects the realizable bandwidths of the current control loop, which subsequently limits the outer control loops. Therefore, pushing for highest possible bandwidths relative to the switching frequency is often a design criterion. One way of achieving that is the implementation of MS-MU-PWM.

Using describing function approach, small-signal model of the multisampled PWM with triangular carrier is found to be almost equal to a pure delay of $\frac{T_c}{2}$, where T_c is the modulating waveform update period [13]

$$G_{DPWM}(s) = \frac{d(s)}{m(s)} = A(\omega, D, N_c)e^{-s\frac{T_c}{2}}, \quad (1)$$

where s is the complex variable of the Laplace transform, d is the continuous-time duty cycle used for averaged modeling, ω is the angular frequency, and D is the steady-state duty cycle. The gain A can be approximated with unity gain with negligible losses in modeling accuracy [13]. In DSP applications, update of the modulating waveform is usually delayed by one control period T_c, due to the non-negligible computational time [11]. This update delay can be represented in s-domain as:

$$G_{ud}(s) = e^{-sT_c}. \quad (2)$$

Combining delays due to modulation (1) and algorithm computation (2) results in total digital delay being equal to:

$$\tau_d = \frac{3}{2}T_c = \frac{3}{2}\frac{T_{pwm}}{N_c}. \quad (3)$$

From (3), it can be seen that multi-update control reduces digital delays inversely to the multi-update factor N_c. Traditionally, double-update is the most often used method, which results in twice decreased delays compared to single-update. The term multisampled (multi-update) control is most often used when N_c is increased above 2. This kind of control is a promising way of bringing the digital control close to analog regarding achievable bandwidths. However, care must be taken as significant nonlinearities are also introduced in the control system, mainly due to the discontinuity of the modulating waveform, which now features switching ripple component as well. For this reason, multi-update control is most often followed by feedback filtering, which entirely removes the switching ripple from the feedback signal. Note that the discontinuity problems are strongly suppressed at high values of multi-update rate [13].

B. Discrete-time model of a three-phase RL load

Given the simplicity of the inverter topology with a RL load, its model can be easily derived directly in discrete-time domain, which is suitable for the design of digital controllers. Note that for direct-discrete modeling, the action of the PWM is assumed to be equal to a zero-order hold in stationary $\alpha\beta$ frame:

$$G_{DPWM,\alpha\beta} \approx \frac{1 - e^{-sT_c}}{s}. \tag{4}$$

While the exact model is shown in (1), for the very specific case of triangular carrier, MS-PWM can still be well-approximated with a ZOH with the update rate equal to f_c.

The direct discrete-time modeling can be found in [5]–[7]. This paper follows the procedure from [7]. In order to analyze the three-phase RL load as single-input single-output (SISO) system, complex variables are used. Starting from the $\alpha\beta$ frame, the differential equations necessary for modeling are:

$$\underline{u}_{\alpha\beta}(t) = R\underline{i}_{\alpha\beta}(t) + L\frac{d}{dt}\underline{i}_{\alpha\beta}(t), \tag{5}$$

where R and L are the line resistance and the line inductance, respectively. The machine back-emf or the grid voltage is neglected in this analysis, as the paper does not take into account the disturbance rejection. The s-domain transfer function from applied voltage to the line current, corresponding to (5) is:

$$G_{i,\alpha\beta} = \frac{1}{R}\frac{1}{1 + s\frac{L}{R}}. \tag{6}$$

Multiplication of (2), (4) and (6) yields the plant model in $\alpha\beta$ frame. The transformation from $\alpha\beta$ to dq frame is obtained using the substitution $s \to s + j\omega_o$, where ω_o is the dq frame rotating frequency. This yields the following s-domain plant transfer function in dq frame:

$$G_{p,dq}(s) = e^{-(s+j\omega_o)T_c}\frac{1 - e^{-(s+j\omega_o)T_c}}{s + j\omega_o}\frac{1}{R}\frac{1}{1 + s\frac{L}{R} + j\omega_o\frac{L}{R}}. \tag{7}$$

The discrete-time model is obtained directly from (7) using $\mathcal{Z}$ transform table:
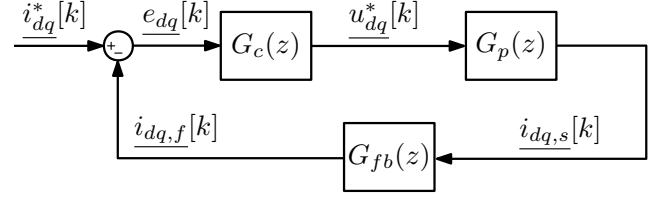

Fig. 2: Small-signal block diagram of the system from Fig. 1 in discrete-time domain.

$$G_{p,dq}(z) = \frac{\left(1 - e^{-\frac{R}{L}T_c}\right)e^{-2j\omega_oT_c}}{R}\frac{1}{z\left(z - e^{-\left(\frac{R}{L}+j\omega_o\right)T_c}\right)}, \tag{8}$$

where z is the complex variable of the $\mathcal{Z}$ transform.

The model obtained in (8) is used for the subsequent derivation of the model-based controller.

C. Discrete IMC controller

The dq frame discrete-time small signal block diagram of the control system in Fig. 1 is shown in Fig. 2. The IMC controller is derived by inverting the plant model and adding an integrator with gain α that determines the crossover frequency [6]. For the sake of causality, due to digital delays, additional factor of $\frac{1}{z^2}$ is added to the controller structure, which results in the following transfer function:

$$G_c(z) = \frac{\alpha \cdot z}{z - 1}\frac{1}{z^2}G_{p,dq}^{-1}(z) = \frac{\alpha \cdot R \cdot e^{j\omega_oT_c}}{\left(1 - e^{-\frac{R}{L}T_c}\right)}\frac{ze^{j\omega_oT_c} - e^{-\frac{R}{L}T_c}}{z - 1}. \tag{9}$$

By implementing the controller from (9) without any feedback filters, the following open-loop transfer function is obtained:

$$W_{ol,1}(z) = G_c(z)G_p(z) = \frac{\alpha}{z(z - 1)} \tag{10}$$

In [6] it is shown that relying on two samples per T_{pwm} often results in unacceptable feedback signal deterioration in industrial applications. This is due to the unalignment between the voltage impulse and sampling instants due to limited current sensor bandwidths, analog feedback filters, delays in driver circuits, and similar. Furthermore, the feedback signal often comprises oscillations due to the LC parasitics of long cables that are present in industrial drives. This is a motivation behind the implementation of MS-DU-PWM in [6] and MS-MU-PWM in this paper, where the signal is highly oversampled and then averaged over the switching period.

III. FEEDBACK ACQUISITION, COORDINATE FRAME TRANSFORMATION, AND FILTERING

A. Feedback acquisition and $\alpha\beta - dq$ transformation

The timing diagram of feedback acquisition, coordinate frame transformation and controller update is shown in Fig. 3. The modulating waveform is illustrated for one phase, $m_a(t)$. The digital system analyzed in this paper features two
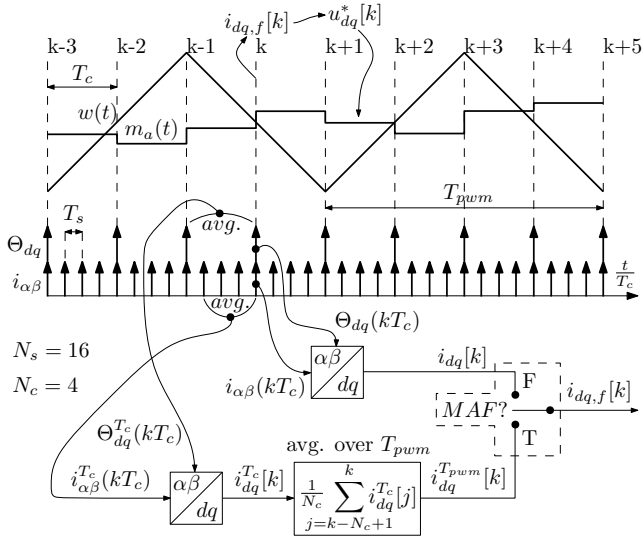
Fig. 3: Timing illustration for signal acquisition, filtering, and modulating waveform update. The position of the selector $MAF?$ determines whether the feedback currents are obtained without filtering or using one switching period averaging. The figure is given for $N_s = 16$ and $N_c = 4$.

independent frequencies. First one is the control frequency, which defines the controller execution rate and update of the modulating waveform. It is defined by the multi-update factor N_c. Control interrupts over the switching period are synchronized with the carrier $w(t)$ such that the first one occurs when the carrier is equal to 0 while other $N_c - 1$ are delayed by T_c each. The second frequency is the sampling frequency, which is defined by the multisampling factor N_s. This allows the DSP to acquire the signal with much higher rate than it can calculate the control algorithm, by employing the standardly available DMA module. High sampling rates allow the use of digital filters, for example MAFs, and subsequent decimation to provide the feedback $i_{dq,f}[k]$ at the control execution rate. Again, sampling instants are synchronized with the carrier such that the first one occurs when the carrier is equal to 0.

Fig. 3 is given for $N_c = 4$ and $N_s = 16$. At instant kT_c, dq frame feedback current $i_{dq,f}[k]$ is obtained and used to calculate the voltage reference $u_{dq}^*[k]$, which is used to calculate the segment of the modulating waveform that is applied at the beginning of the following control interrupt. The synchronous frame signal Θ_{dq} is obtained each T_c by implementing a PLL or using resolver/encoder sensors.

As shown in Fig. 3, the selector $MAF?$ chooses whether the feedback is provided without any filtering, or using a MAF over the switching period. In the first case, the latest samples of $i_{\alpha\beta}(kT_c)$ and $\Theta_{dq}(kT_c)$ are used to obtain the dq frame current $i_{dq}[k]$, which is used as the feedback signal. In case when $N_c = N_s = 2$, we obtain the standardly used DS-DU control. In cases when $N_c = N_s > 2$, we obtain the MS-MU-PWM with switching ripple in the feedback signal [12].

In cases when the MAF is used, the goal is to obtain a true average value of dq currents over one switching period. The

$\alpha\beta$ currents are first averaged over T_c, using $\frac{N_s}{N_c}$ latest current samples, to obtain $i_{\alpha\beta}^{T_c}(kT_c)$. This average current is then transformed to dq frame to obtain $i_{dq}^{T_c}[k]$. The transformation is performed using the angle $\overline{\Theta}_{dq}^{T_c}(kT_c)$, calculated as an average of two latest angle values. If $N_c \geq 2$, currents are further averaged using N_c values of $i_{dq}^{T_c}$ to obtain the average value during the previous switching period $i_{dq}^{T_{pwm}}[k]$. For this filtering strategy, in cases when $N_s > N_c = 2$, we obtain MS-DU control, where the filtering is used to obtain a true-average value at the expense of reduced system dynamics [6]. In cases when $N_s \geq N_c > 2$, we obtain MS-MU-PWM control with switching ripple being filtered from the feedback signal. The factor N_s is chosen to be as high as allowed by the maximal ADC sampling rate. Note that independently of whether the MAF is used or not, transformation of the reference voltage from dq to $\alpha\beta$ frame, shown in Fig. 1, is always performed with the latest value of the angle $\Theta_{dq}(kT_c)$.

B. Total time delay in DSP application

For control loop analysis and comparison between DS-DU-PWM, MS-DU-PWM, and MS-MU-PWM based on the crossover frequency and phase margin it is of interest to analyze the loop delays in continuous-time domain.

The equivalent time delay of the algorithm calculation and the DPWM modulation is shown in (3). For DS-DU-PWM without any feedback filtering, this corresponds to the total delay:

$$\tau_{d,DS-DU} = \frac{3}{2}\frac{T_{pwm}}{2}. \tag{11}$$

For MS-DU-PWM, the MAF is most often used to filter out the switching frequency component. The phase lag of the MAF over T_{pwm} can be closely approximated by a pure delay equal to $\frac{T_{pwm}}{2}$. This results in the equivalent time-delay:

$$\tau_{d,MS-DU,MAF} = \frac{3}{2}\frac{T_{pwm}}{2} + \frac{T_{pwm}}{2} = \frac{5}{4}T_{pwm}. \tag{12}$$

For MS-MU-PWM without MAF, equivalent time-delay is equal to (3). Finally, for MS-MU-PWM with MAF, equivalent time-delay is:

$$\tau_{d,MS-MU,MAF} = \frac{3}{2}\frac{T_{pwm}}{N_c} + \frac{T_{pwm}}{2} = \frac{\frac{3}{N_c} + 1}{2}T_{pwm}. \tag{13}$$

The MS-DU-PWM features significant time-delay due to MAF and high modulating and control delays. For high dynamic performance, MS-DU-PWM controller structure needs to include additional derivative gain compared to (9), to compensate for the high delays [6]. Regarding dynamics, best case is represented by the MS-MU-PWM without MAF. For multi-update factors $N_c \geq 8$, control delays are practically removed and dynamic capabilities become equal to the ones of analog controllers. Finally, from (13) it can be seen that for MS-MU-PWM with a MAF, starting from $N_c > 6$, equivalent time delay is lower than for the DS-DU-PWM. This is important as it states that the same kind of filtering as in MS-DU-PWM can be used to obtain a high quality feedback signal, while

the dynamic is improved instead of deteriorated compared to standardly used DS-DU-PWM.

IV. CONTROLLER PARAMETER DESIGN

For the purpose of controller tuning, the analysis is performed in discrete-time domain, with a rate equal to f_c. For this purpose, even if $N_s > N_c$, the MAF is approximated as a filter at frequency f_c using the following transfer function [6]:

$$G_{MAF}(z) = \frac{1 + 2z^{-\frac{N_c}{2}} + z^{-N_c}}{4}. \tag{14}$$

For the tested methods that do not use the feedback filter, the open-loop transfer function is given in (10). For methods that use the MAF, the open loop transfer function is equal to:

$$W_{ol,2}(z) = W_{ol,1}(z)G_{MAF}(z) \tag{15}$$

For a clear dynamic comparison, the controller gain α in (9) is set such that the phase margin equal to 70° is achieved for all tested methods. In this way, the crossover frequency is increased for methods with a lower equivalent time delay. In this paper, the verification is performed on a BLDC motor, with parameters shown in Table I:

TABLE I: Machine and Inverter Parameters

BLDC motor	value	unit	
Number of poles	$2p$	6	/
Rated torque	T_{nom}	6	Nm
Rated current	I_{nom}	7.3	A_{rms}
Torque constant	k_t	0.821	$Nm/(A_{rms})$
Back-EMF constant	k_e	1.2534	$V_{peak}/(rad/s)$
Stator resistance	R_s	0.47	Ω
Stator inductance	L_s	3.4	mH
Inverter	value	unit	
DC link voltage	U_{dc}	520	V
Switching frequency	f_{pwm}	10	kHz
Dead time	t_{dt}	1	μs

The first tested strategy is the standardly used DS-DU approach. For a 70° phase margin, the value of α is equal to 0.23 and the achieved crossover frequency is equal to $7.3\% f_{pwm}$. The second tested strategy is the MS-DU control with the oversampled MAF in the feedback path. The controller gain α is equal to 0.14, which sets the crossover frequency to $4.4\% f_{pwm}$. Finally, the gain α of the proposed MS-MU method with a MAF based feedback acquisition is equal to 0.0636, which sets the crossover frequency to $8\% f_{pwm}$. The MS-MU-PWM without ripple filtering is not implemented, as the discontinuity impact in three-phase applications is still not properly investigated. For both MS-DU and MS-MU, the multisampling ratio is set to $N_s = 16$. For MS-MU, the multi-update ratio is chosen as $N_c = 8$, which was limited by the algorithm execution time on the used DSP.

The closed-loop -3 dB bandwidth is calculated using $W_{cl,1}(z) = \frac{W_{ol,1}(z)}{1+W_{ol,1}(z)}$ for the case of DS-DU and $W_{cl,2}(z) =$ $\frac{G_c(z)G_p(z)}{1+W_{ol,2}(z)}$ for the case of MS-DU and MS-MU. The summary of control loop parameters are shown in Table II. It can be seen that the MS-MU with the MAF achieves better dynamics than the DS-DU.

TABLE II: Control loop parameters

DS-DU	label	value	unit
IMC gain	α	0.23	/
Cross-over frequency	f_c	735	Hz
Phase margin	pm	70.2	$^\circ$
Closed-loop bandwidth	f_{bw}	1253	Hz
MS-DU with MAF, $N_s = 16$	label	value	unit
IMC gain	α	0.14	/
Cross-over frequency	f_c	445	Hz
Phase margin	pm	70	$^\circ$
Closed-loop bandwidth	f_{bw}	766	Hz
MS-MU with MAF, $N_s = 16$, $N_c = 8$	label	value	unit
IMC gain	α	0.0636	/
Cross-over frequency	f_c	799	Hz
Phase margin	pm	70.3	$^\circ$
Closed-loop bandwidth	f_{bw}	1387	kHz

A. Verification of discrete-time modelling

For proposed MS-MU with MAF, simulations in MATLAB/Simulink were performed in order to verify the discrete-time modeling. The sweep frequency response analysis (SFRA) is performed to verify the open-loop transfer function (15) for parameters in Table I Table II. In simulations, a detailed model of the DPWM, which resembles the action qualifier module realization within the DSP TI f28379d EPWM peripheral, is implemented. The motor is modeled in the continuous-time domain using the Simulink abc frame machine model. The motor speed is set to 565 rpm, which results in the output frequency $f_o = 270$ Hz. For the measured axis response, the perturbation magnitude is set to 0.1 A, while for the other axis the controller input is set to 0. The perturbation frequencies are an arithmetic sequence from 400 Hz to 5000 Hz, with a step of 230 Hz. The axis open loop SFRA result is shown in Fig. 4. The simulated results are compared to the analytics and it can be seen that a very good match is achieved.

V. EXPERIMENTAL VERIFICATION

This section provides the experimental validation of the previously discussed controllers using the Typhoon HIL 402 platform and DSP TI f28379d. Power stage is implemented within hardware-in-the-loop (HIL) simulation model and comprises DC voltage source, IGBT inverter and BLDC motor with parameters from Table I. The motor line currents are obtained via HIL's analog outputs and are routed to DSP's ADC inputs. The motor angle information is obtained using the encoder signals, which are sent from HIL's digital outputs to the DSP's QEP inputs. These current and position feedback
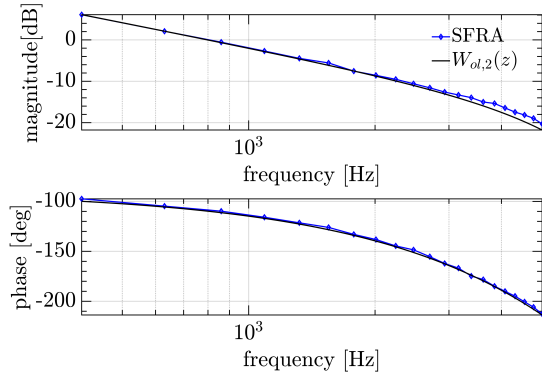
Fig. 4: Simulated SFRA results for open-loop system with the MS-MU control strategy. The drive parameters are shown in Table I and the controller parameters are shown in Table II. The results are compared with the analytic frequency response of $W_{ol,2}(z)$

Fig. 5: Verification of a q-axis step response for DS-DU control strategy. The drive parameters are shown in Table I and the controller parameters are shown in Table II. The results are compared with the analytical step response of $W_{cl,1}(z)$. The d-axis current is shown to demonstrate decoupling capabilities.

Fig. 6: Verification of a q-axis step response for MS-DU control strategy. The drive parameters are shown in Table I and the controller parameters are shown in Table II. The results are compared with the analytical step response of $W_{cl,2}(z)$. The d-axis current is shown to demonstrate decoupling capabilities.

Fig. 7: Verification of a q-axis step response for MS-MU control strategy. The drive parameters are shown in Table I and the controller parameters are shown in Table II. The results are compared with the analytical step response of $W_{cl,2}(z)$. The d-axis current is shown to demonstrate decoupling capabilities.

signals are used to perform the FOC algorithm in the DSP in the same way as described in Section III. The resulting gate signals are sent from DSP's EPWM outputs to HIL's digital inputs. Note that a particular logic had to be implemented in the DSP algorithm, in order to allow the implementation of MS-PWM without the occurrence of pulse-skipping. Namely, the used DSP from TI modifies the PWM output when the modulating waveform is strictly equal to the carrier's counter value. This prevents the detection of vertical crossings [13], which results in full or zero duty cycle. The situation comprising a vertical crossing is illustrated in Fig. 3 at the instant kT_c. This prolongs the execution time, but still allows the complete FOC algorithm to run at $N_c = 8$ and $f_{pwm} = 10$ kHz.

For each of the control strategies analyzed in Section IV, HIL simulations were performed to obtain q-axis current step responses and compare them to the step response of the corresponding closed loop transfer functions $W_{cl,1}$ and $W_{cl,2}$. The motor speed is set to 565 rpm, which results in the output frequency $f_o = 270$ Hz. Step responses are shown in Fig. 5-7. Note that the presented HIL results are obtained by post processing of the signals exported from DSP's RAM. The dq domain currents are acquired each T_s and the angle is acquired each T_c. For visualization and comparison with the analytics, the switching ripple is removed using the same filtering approach as in Fig. 3, however in a non-causal manner so that delays are not added. According to the presented results there is a very good match between experimental and analytical results for all compared control strategies. DC error which is visible in case of DS-DU controller (Fig. 5) is due to the aliasing present as a consequence of the delay introduced by HIL (approximately 2.5 us). This delay prevents the sampling instant to coincide with the middle of the current ripple. Note that this error can be compensated by offsetting the sampling instant, however, it was of interest to emphasize this drawback of the control methods that rely only on two samples per switching period.
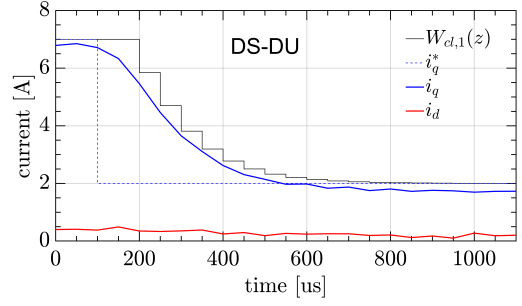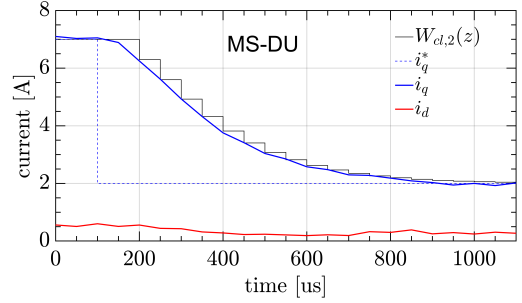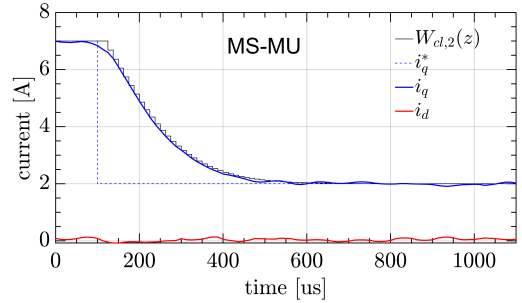
VI. CONCLUSIONS

This paper has presented a multisampled multi-update (MS-MU-PWM) current control strategy applied to a high-speed three-phase electric drive. The independent choice of sampling and control-update frequencies allows the high-quality feedback acquisition with improved dynamic capabilities compared to the standard double-update method. The analysis is verified using a DSP TI f28379d and a Typhoon HIL 402 hardware-in-the-loop system.

References

[1] D. G. Holmes, B. P. McGrath, and S. G. Parker, "Current regulation strategies for vector-controlled induction motor drives," *IEEE Transactions on Industrial Electronics*, vol. 59, no. 10, pp. 3680–3689, 2012.

[2] J. Yim, S. Sul, B. Bae, N. R. Patel, and S. Hiti, "Modified current control schemes for high-performance permanent-magnet ac drives with low sampling to operating frequency ratio," *IEEE Transactions on Industry Applications*, vol. 45, no. 2, pp. 763–771, 2009.

[3] I. Z. Petric, S. N. Vukosavic, M. Degano, and A. Galassini, "A digital internal model current controller for salient machines," *IEEE Transactions on Industrial Electronics*, vol. 68, no. 6, pp. 4703–4717, 2021.

[4] A. G. Yepes, A. Vidal, J. Malvar, O. López, and J. Doval-Gandoy, "Tuning method aimed at optimized settling time and overshoot for synchronous proportional-integral current control in electric machines," *IEEE Transactions on Power Electronics*, vol. 29, no. 6, pp. 3041–3054, 2014.

[5] H. Kim, M. W. Degner, J. M. Guerrero, F. Briz, and R. D. Lorenz, "Discrete-time current regulator design for ac machine drives," *IEEE Transactions on Industry Applications*, vol. 46, no. 4, pp. 1425–1435, 2010.

[6] S. N. Vukosavić, L. S. Perić, and E. Levi, "Ac current controller with error-free feedback acquisition system," *IEEE Transactions on Energy Conversion*, vol. 31, no. 1, pp. 381–391, 2016.

[7] C. A. Busada, S. G. Jorge, and J. A. Solsona, "Comments on "digital current control in a rotating reference frame—part i: System modeling and the discrete time-domain current controller with improved decoupling capabilities"," *IEEE Transactions on Power Electronics*, vol. 34, no. 3, pp. 2980–2984, 2019.

[8] L. Rovere, A. Formentini, and P. Zanchetta, "Fpga implementation of a novel oversampling deadbeat controller for pmsm drives," *IEEE Transactions on Industrial Electronics*, vol. 66, no. 5, pp. 3731–3741, 2019.

[9] C. Xu, Z. Han, and S. Lu, "Deadbeat predictive current control for permanent magnet synchronous machines with closed-form error compensation," *IEEE Transactions on Power Electronics*, vol. 35, no. 5, pp. 5018–5030, 2020.

[10] K. Ito, R. Suzuki, K. Yoshimoto, and T. Yokoyama, "A study of multisampling deadbeat control for low carrier frequency pmsm drive system used in evs and hevs," in *2021 IEEE International Conference on Mechatronics (ICM)*, 2021, pp. 1–6.

[11] S. Buso and P. Mattavelli, "Digital control in power electronics, 2nd edition," *Synthesis Lectures on Power Electronics*, Morgan & Claypool Publishers, USA, 2015.

[12] I. Z. Petric, P. Mattavelli, and S. Buso, "Noise attenuation properties of multisampled control in power electronics," in *2020 IEEE 21st Workshop on Control and Modeling for Power Electronics (COMPEL)*, 2020, pp. 1–6.

[13] L. Corradini and P. Mattavelli, "Modeling of multisampled pulse width modulators for digitally controlled dc–dc converters," *IEEE Transactions on Power Electronics*, vol. 23, no. 4, pp. 1839–1847, 2008.

[14] L. Corradini, W. Stefanutti, and P. Mattavelli, "Analysis of multisampled current control for active filters," *IEEE Transactions on Industry Applications*, vol. 44, no. 6, pp. 1785–1794, 2008.

[15] C. Restrepo, T. Konjedic, F. Flores-Bahamonde, E. Vidal-Idiarte, J. Calvente, and R. Giral, "Multisampled digital average current controls of the versatile buck–boost converter," *IEEE Journal of Emerging and Selected Topics in Power Electronics*, vol. 7, no. 2, pp. 879–890, 2019.

[16] I. Petric, P. Mattavelli, and S. Buso, "A jitter amplification phenomenon in multisampled digital control of power converters," *IEEE Transactions on Power Electronics*, pp. 1–1, 2021.

[17] S. He, D. Zhou, X. Wang, and F. Blaabjerg, "Aliasing suppression of multi-sampled current controlled lcl-filtered inverters," *IEEE Journal of Emerging and Selected Topics in Power Electronics*, pp. 1–1, 2021.

[18] S. Buso, T. Caldognetto, and D. I. Brandao, "Dead-beat current controller for voltage-source converters with improved large-signal response," *IEEE Transactions on Industry Applications*, vol. 52, no. 2, pp. 1588–1596, 2016.